Laura C. Folkers*, Laura Teresa Corredor, Fabian Lukas, Manaswini Sahoo, Anja U. B. Wolter and Anna Isaeva

Occupancy disorder in the magnetic topological insulator candidate $Mn_{1-x}Sb_{2+x}Te_4$

https://doi.org/10.1515/zkri-2021-2057
Received October 7, 2021; accepted November 26, 2021;
published online December 28, 2021

Abstract: $MnSb_2Te_4$ is a candidate magnetic topological insulator exhibiting more pronounced cation intermixing than its predecessor $MnBi_2Te_4$. Investigating the cation intermixing and its possible implications on the magnetic order in $MnSb_2Te_4$ are currently hot topics in research on quantum materials for spintronics and energy-saving applications. Two single-crystal X-ray diffraction measurements of $Mn_{1-x}Sb_{2+x}Te_4$ (x = 0.06 and x = −0.1) are presented alongside a detailed discussion of its crystal structure with a spotlight on the apparent occupancy disorder between the two cations. This disorder has been noted by other groups as well, yet never been analyzed in-depth with single-crystal X-ray diffraction. The latter is the tool of choice to receive a meaningful quantification of antisite disorder. Between the two synthesis procedures we find subtle differences in phases and/or alternation of the cation content which has implications on the magnetic order, as illustrated by bulk magnetometry. Understanding and assessing this disorder in magnetic topological insulators of the MnX_2Te_4 (X = Bi, Sb) type is crucial to gauge their applicability for modern spintronics. Furthermore, it opens new ways to tune the "chemical composition – physical property" relationship in these compounds, creating an alluring aspect also for fundamental science.

Keywords: magnetic topological materials; magnetism; single crystal X-ray diffraction; site disorder.

1 Introduction

Today's materials science is driven by the pursuit of novel functional materials to allow for e.g. the ongoing development of computing and energy-saving technologies. These functional materials encompass for instance multiferroics, high-temperature superconductors and topologically non-trivial materials, i.e. materials exhibiting unconventional combinations of electronic conductivity and magnetism. Our interest lies in the pursuit of topological materials, which allow for a dissipationless spin transport on their surfaces, that is not disturbed by structural imperfections or inclusions [1–3].

Two archetypes of topological insulators that stimulated an excessive amount of research in the last few years, Bi_2Te_3 and Sb_2Te_3, exhibit the tetradymite-type (Bi_2STe_2) [4] crystal structure, i.e. they both crystallize in the rhombohedral $R\bar{3}m$ space group and are built of Te–Bi–Te–Bi–Te quintuple layers which are formed by [$BiTe_6$] octahedra. The current even hotter than hot topic is to combine long-range magnetic order – a bulk property – with the topologically protected transport – a surface property – and have them influence each other. This has been first achieved in $Cr_x(Bi,Sb)_2Te_3$, which was the artificial heterostructure on which the quantum anomalous hall effect (QAHE) was discovered [5]. Ongoing pursuit of intrinsic magnetic topological materials, both insulators and semimetals, has yielded a handful of promising candidates, including $EuIn_2As_2$ [6], CuMnAs [7] and $TbMn_6Sn_6$ [8]. In the case of tetradymite-based compounds magnetic order could be introduced intrinsically by adding Mn^{2+} to the structure, resulting in the intrinsic magnetic topological insulator (IMTI) $MnBi_2Te_4$ [9, 10]. In contrast to Bi_2Te_3 and Sb_2Te_3, this layered compound is built of septuple Te–Bi–Te–Mn–Te–Bi–Te layers, which also form octahedra [$BiTe_6$] and [$MnTe_6$].

Laura C. Folkers and Laura Teresa Corredor contributed equally to the article.

***Corresponding author: Laura C. Folkers,** Institute for Solid State and Materials Physics, Technische Universität Dresden, Dresden, Germany; Leibniz Institute for Solid State and Materials Research Dresden, Dresden, Germany; and ct.qmat Dresden and Würzburg Cluster of Excellence, Dresden, Germany
E-mail: laura_christina.folkers1@tu-dresden.de
Laura Teresa Corredor, Manaswini Sahoo and Anja U. B. Wolter, Leibniz Institute for Solid State and Materials Research Dresden, Dresden, Germany
Fabian Lukas, Technische Universität Dresden; and Leibniz Institute for Solid State and Materials Research Dresden, Dresden, Germany
Anna Isaeva, Leibniz Institute for Solid State and Materials Research Dresden, Dresden, Germany; and Van der Waals-Zeeman Instituut, University of Amsterdam, Dresden, Germany

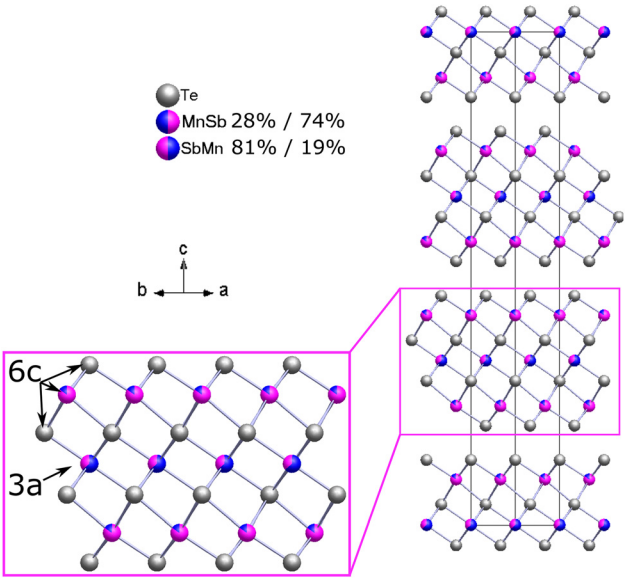

Figure 1: The average unit cell of $MnSb_2Te_4$ exhibiting the typical septuple layers including the occupancy disorder. One of the septuple layers is enlarged for better visibility.

Our group developed the first growth protocol and characterized single crystals of $MnBi_2Te_4$ [10], which display ferromagnetic (FM) coupling within a layer of manganese and antiferromagnetic (AFM) order between the respective layers (see Figure 1 which shows the layers of Mn on the example of $MnSb_2Te_4$). Moreover, the QAHE could be achieved in thin exfoliated flakes of $MnBi_2Te_4$ under an external magnetic field of 12 T that fully polarized the lattice into a ferromagnet [11]. For QAHE stable at high temperatures and lower magnetic fields (ideally, without any external field), a ferromagnetic bulk magnetic order is highly desirable.

MnSb $_2Te_4$ is a new isostructural analogue that has rapidly gained interest in the community [12–17]. Opposed to $MnBi_2Te_4$, various magnetic behaviors have been reported for $MnSb_2Te_4$ ranging from a bulk antiferromagnet to a ferri- or ferromagnet [12–19]. Its synthesis procedures seem to vary greatly between the reports and presumably influence the type of the magnetic order. As outlined in ref. [13], these effects may be connected via the cation intermixing phenomenon. When intermixing is accounted for, Mn is not only found in the center of the septuple layer, but also in the outer cationic positions. Equally, some Sb is populating the central Mn position, leading to some occupancy disorder. Since Mn^{2+} carries a magnetic moment (d^5 state), its amounts and placements within the unit cell have a decisive impact on the magnetic exchange coupling and magnetic order in $MnSb_2Te_4$. This intermixing is easiest characterized with single crystal X-ray diffraction as this method is more precise than powder diffraction and depicts a larger sample volume than electron microscopy or tunneling spectroscopy. In our previous work [10], similar cation disorder has been for the first time characterized for $MnBi_2Te_4$. The present study explores the Mn/Sb intermixing in two distinct $Mn_{1-x}Sb_{2+x}Te_4$ crystals and its implications for magnetism.

2 Experimental

Single crystalline specimens were produced via a solid state reaction. Sample 1 (S1) was prepared by tempering stoichiometric amounts of MnTe and Sb_2Te_3 at 630 °C in an evacuated quartz tube for 10 days and subsequent quenching in water. Sample 2 (S2) was synthesized from the elements with a 10% smaller amount of Te, than demanded by stoichiometry, in a quartz ampule sealed off under vacuum. It was tempered at 594 °C for three days, and subsequently quenched in water. The ovens used for these experiments were custom built two-zone ovens (Reetz GmbH) with two free moving thermocouples. Those thermocouples were placed directly next to the quartz ampule which contained the sample, allowing for temperature control as precise as ±1 K. After quenching the ampules contained ingots of solidified melt that were cracked open to give two types of samples. On one hand the resulting metallic crumbs were either ground for powder diffraction or pressed to pellets for magnetic measurements. On the other hand the crumbs were inspected through an optical microscope and flat specimens with mirror-like surfaces were selected for single-crystal diffraction and energy dispersive X-ray spectroscopy.

The respective crystals (denoted as S1 and S2 in the text, just as the respective bulk specimens) were measured on a Rigaku Supernova four circle diffractometer, fitted with a molybdenum tube and an AtlasS2 detector. The data was subsequently indexed and integrated in the respective diffractometer software CrysAlisPro [20] and the crystal structures were solved and refined with Superflip [21] and Jana2006 [22]. Upon inspection of reciprocal space reconstructions neither data set showed any sign of diffuse scattering or super structure reflections.

The average structure was solved and refined without any special tricks. To allow for some Sb to populate the 3*a* position and some Mn to populate the 6*c* position (see Figure 1), both positions were split and populated with 50% Mn and 50% Sb. Furthermore both positions were restrained so that the ADP parameters and coordinates were identical and the occupancies would keep the overall sum of the respective position. When this setup proved stable, the occupancies of Mn and Sb were allowed to refine, while still keeping the above restraints. In a last step, the restraint of the occupancy having to sum up to the site multiplicity was lifted, to allow for the possibility of voids. However neither of the samples showed any significant change of occupancies after this, indicating that no vacancies could be found in our data sets. As a consequence our refined compositions are electroneutral.

Sample 1 additionally shows a small amount (twin volume 2 = 1%) of twinning, which was treated in Jana2006 by a 180° rotation around the *b*-axis (0, 1, 0) in reciprocal space. Also S2 exhibits twinning that could be directly treated in Jana2006 through a 60° rotation around the *c*-axis (0, 0, 1) in reciprocal space. Twin 1 accounts for 29% of the data while twin 2 accounts for 71% of the data (see Supplementary Figure 3). The last few cycles of the refinement were performed on F^2. Powder X-ray diffraction (PXRD) measurements were conducted on a Malvern Panalytical Empyrean 3 diffractometer, fitted

with a copper tube and set in Bragg-Brentano geometry. Simple Le Bail decompositions against literature data were performed in JANA2006 [22] to check for phase purity. See Supplementary Figures 1 and 2. Energy-dispersive X-ray spectroscopy (EDX) was conducted on a Hitachi FESEM SU 8020 microscope equipped with a Silicon Drift Detector (SDD) X-Max^N (Oxford) at an acceleration voltage of 20 kV and a current of 5 μA. Flat platelet crystalline samples were prepared on a sticky carbon film.

Magnetization measurements were conducted with a commercial Quantum Design superconducting quantum interference device magnetometer (SQUID-VSM) on pressed powder pellets.

3 Structural studies

$MnSb_2Te_4$ crystallizes in the $R\bar{3}m$ (No. 166) space group, with average lattice parameters a = 4.2 Å and c = 40.8 Å (for more details see Table 1). This structure is built of septuple-layer slabs which are interleaved by a van der Waals gap. The septuple slabs are in turn built of stacks of Te–Sb–Te–Mn–Te–Sb–Te, each layer stretching out infinitely in the *ab* plane (Figure 1). In the unit cell Mn is located on the Wyckoff position 3*a* (0, 0, 0), while the other atoms are situated on 6*c* Wyckoff positions.

Table 1: Structural information for Sample 1 and Sample 2 of $Mn_{1-x}Sb_{2+x}Te_4$.

	Sample 1	Sample 2
Refined composition	$Mn_{1.11(2)}Sb_{1.90(2)}Te_4$	$Mn_{0.94(2)}Sb_{2.07(2)}Te_4$
Formula weight (g/mol)	803.20	813.70
Crystal size (mm^3)	0.06 × 0.05 × 0.01	0.1 × 0.06 × 0.03
Color	Metallic grey	
Crystal system	Rhombohedral	
Space group	$R\bar{3}m$ (No. 166)	
Lattice parameters (Å)	a = 4.2329(1)	a = 4.2471(1),
	c = 40.8387(7)	c = 40.8927(7)
Cell angles	$\alpha = \beta = 90°$, $\gamma = 120°$	
Formula units (Z)	3	
R_{int} (%)	4.7	7.1
R_{obs} (%)	3.15	3.89
wR_{obs} (%)	10.10	15.25
GOF (all)	1.96	1.91
Max. residual density ($e \times 10^{-6}$ pm^{-3})	4.52	8.43
Min. residual density ($e \times 10^{-6}$ pm^{-3})	−3.37	−8.62
No. of parameters	15	17
No of constraints	5	3
No. of unique reflections	390	399
2Theta max. (°)	34.1	34.21
2Theta min. (°)	2.99	2.99
CCDC No.	2107053	2107055

In the parent compound $MnBi_2Te_4$, a certain amount of intermixing between the cationic sites was established previously [10, 23, 24] with the compositions and magnetic transition temperatures noted in Table 2. Additionally, in this work we have grown and elucidated a $MnBi_2Te_4$ crystal following [10] in order to check possible variations of stoichiometry. The present results are very consistent with the previous findings (see Supplementary Material and Table 2), hinting at a well-defined yet non-stoichiometric composition of the Bi analogue. Therefore intermixing between Mn and Sb was also allowed in our analyses of $MnSb_2Te_4$. Indeed, as in $MnBi_2Te_4$, Mn could be found on the Sb position (6*c*) as well as Sb could be found on the Mn (3*a*) position (see Figure 1).

We will in the following present two structure elucidations of $MnSb_2Te_4$, both nominally the same phase, yet they show differences that cannot be ignored. For the respective synthesis routes and single crystal refinement strategies please refer to the Experimental section. The crystal denoted as Sample 1 (S1) exhibits 28 ± 1.0% of Sb on the 3*a* position and 19 ± 0.3% Mn on the 6*c* position resulting in the overall composition of $Mn_{1.11(2)}Sb_{1.90(2)}Te_4$. The second crystal from a different batch (S2) shows 37 ± 1.4% of Sb on the 3*a* position and 15 ± 0.5% of Mn on the 6*c* position leading to an overall composition of $Mn_{0.94(2)}Sb_{2.07(2)}Te_4$.

As mentioned in the Experimental section, neither structure shows vacancies, indicating that the total sum of Mn and Sb in the compound is fixed to three. The difference between the two samples lies in the distribution of Mn and Sb over the respective sites resulting in S2 exhibiting an underoccupation on the Mn as compared to the idealized formula $MnSb_2Te_4$, while S1 shows an overoccupation. The most significant difference between S1 and S2 is seen in the

Table 2: Occupancy distribution, measurement types and magnetic transition temperature in $MnBi_2Te_4$ from various sources.

Mn:Bi on 3*a*	Mn:Bi on 6*c*	Measurement type	T_N	Magnetic order	References
74:22	6:94	Single crystal XRD	24.6(5) K	AFM	[10]
82:18	5:95	Single crystal XRD	–	–	This paper
82:18	1:99	Single crystal ND	24 K	AFM	[23]
–	3:97	STM	24.1(2) K	AFM	[24]

The 3*a* position is the central position in the septuple layer slab which is occupied by Mn in the average structure and the 6*c* position is the outer cation position occupied by Bi in the average structure. XRD, X-ray diffraction; ND, neutron diffraction; STM, scanning transmission microscopy; AFM, antiferromagnetic.

occupancy of the central Mn position (3*a*) that is more Mn-rich in S1. A close inspection of Table 1 also exhibits large positive and negative residual densities for both samples. This is due to stacking disorder typical for quasi 2D structures and mixed occupancy refinements not allowing to properly account for small atomic movements.

When comparing the interatomic distances and angles in Table 3 and Figure 2, the most obvious discrepancies that can be found are connected to the central position of the septuple layer slab. In light of the different atomic radii of Mn and Sb (2.05 Å and 2.2 Å, respectively [25]) this is indeed sensible. If we calculate the interatomic distances from the above values (2.075 Å for Mn–Te and 2.15 Å for Sb–Te) and subsequently calculate the respective difference between samples 1 and 2 after accounting for the occupancy percentages, we find the same difference (0.1%) between the calculated values and the values tabulated in Table 3. The differences in angles are also most visible around the central 3*a* position and can be connected to the size differences of Mn and Sb and the respective occupancy differences. A qualitative estimation of the size of the van der Waals gap gives the following values: 2.90 Å for S1 and 2.86 Å for S2.

As always with single crystal studies it is important to keep in mind that they only portray a small fraction of the synthesized batch. To receive clarity on the phase purity and elemental composition of the bulk sample we have performed powder X-ray diffraction (PXRD) and energy dispersive X-ray spectroscopy (EDX) overview analyses. While S1 appears phase pure (cf. Supplementary Figure 1), S2 contains additional phases (cf. Supplementary Figure 2). The main phase is indeed $MnSb_2Te_4$ (ca. 90%) but the sample also contains admixtures of Sb_2Te_3 (ca. 6%) and a small amount of $MnSb_4Te_7$ (ca 4%) (as compared with ref. [26]). The approximate phase fractions in brackets have been deduced from a very preliminary Rietveld refinement

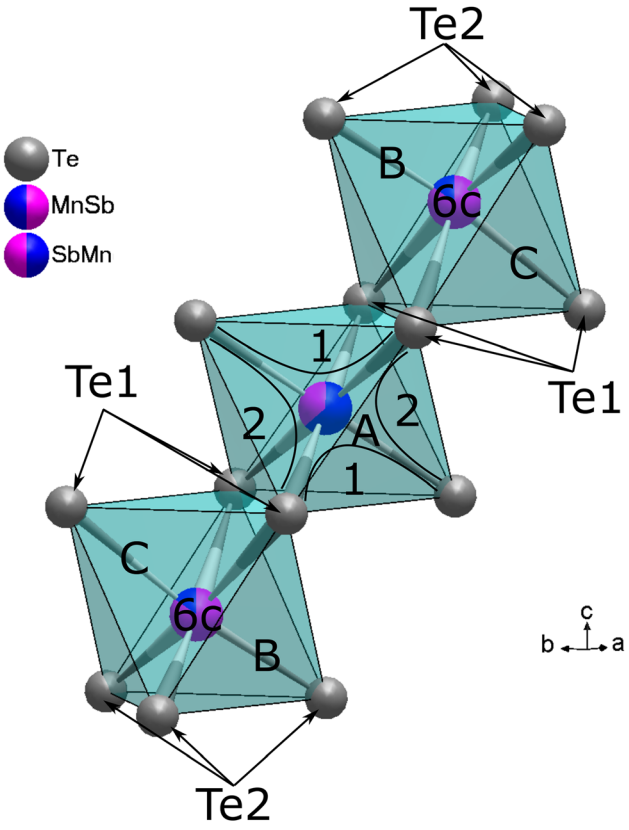

Figure 2: Graphic representation of distances and angles in the [(Mn/Sb)Te_6] octahedra. The figure has been constructed from data of Sample 1 but indicates the respective geometries for both samples.

of the S2 powder data (Supplementary Figure 2) without taking the cationic intermixing into account ($R_p \approx 12\%$; GOF ≈ 3; $R_{obs} \approx 13–20\%$).

EDX analysis of crystallites originating from the S1 batch leads to an average composition of $Mn_{1.06(1)}Sb_{1.95(1)}Te_{4.00(2)}$ which is in good agreement with the refined composition from the single-crystal measurement. Due to its phase purity seen in PXRD this result is not surprising. Contrary to this, the EDX analysis of S2 shows a range of distinct compositions with various percentages of Mn. The 15 data points that can be attributed to the $Mn_{1-x}Sb_{2+x}Te_4$ phase average up to a composition $Mn_{0.96(1)}Sb_{2.14(1)}Te_{4.00(2)}$, which is fairly close to the refined composition of S2 in Table 1. Other elemental compositions found in the S2 batch correspond to ca. 2 at.% of Mn, which could be attributed to Mn-doped Sb_2Te_3, and to 6–7 at.% of Mn, which is characteristic for $MnSb_4Te_7$. This distribution of the EDX results coincides well with the phase mixture elucidated from PXRD. This is a telltale example of how single-crystal diffraction can be deceiving and the entire batch of a sample should always be analyzed with several

Table 3: Shows the interatomic distances and angles as found in the refined structures of sample 1 and sample 2.

Distance/angle	Sample 1	Sample 2	Label
Mn/Sb (3*a*) - Te1	2.9612(1)Å	2.9813(1)Å	A
Mn/Sb (6*c*) - Te1	3.2033(8)Å	3.2089(11)Å	B
Mn/Sb (6*c*) - Te2	2.9292(1)Å	2.9387(1)Å	C
Te1 - Mn/Sb (3*a*) - Te1	91.244(12)°	90.845(15)°	1
Te1 - Mn/Sb (3*a*) - Te1	88.756(12)°	89.155(16)°	2
Te1 - Mn/Sb (6*c*) - Te1	92.52(3)°	92.54(4)°	3
Te1 - Mn/Sb (6*c*) - Te2	92.188(12)°	92.105(17)°	4
Te2 - Mn/Sb (6*c*) - Te2	82.71(2)°	82.87(3)°	5

The last column headed “Label”, connects the distances and angles with their respective positions as indicated by the labels in Figure 2.

Table 4: Magnetic ordering temperatures reported for $MnSb_2Te_4$ in the literature.

$T_{critical}$	Magnetic order	References
34 K	Ferromagnet	[13]
19 K	Antiferromagnet	[12]
25 K	Ferrimagnet	[14]
45–50 K	Ferromagnet	[16]

independent methods. In order to gain solid confidence in our conclusions, we deduced by EDX the elemental composition of the exact single-crystal S2 that was used for the structure refinement: $Mn_{0.83(2)}Sb_{2.28(1)}Te_{4.00(1)}$ as averaged over 10 data points. A stronger deviation from the expected stoichiometry (especially in the Sb:Te ratio) may be connected to an imperfect sample orientation of this tiny crystal.

4 Magnetic studies

One of the central reasons why an in-depth study of the intermixing in $MnSb_2Te_4$ is important, is its impact on the magnetic ordering in these compounds. As alluded to in the introduction, the magnetism found in $MnSb_2Te_4$ differs from $MnBi_2Te_4$ not only by anti-versus ferromagnetism, but also by its robustness. As can be seen in Table 2, the Néel temperature of $T_N \approx 24$ K is very consistent over various measurements on $MnBi_2Te_4$, albeit slight variations of the occupancy values. Hence, there are two points which strongly differ between our $MnBi_2Te_4$ and $MnSb_2Te_4$ samples: 1. The intermixing in our $MnBi_2Te_4$ crystals is reproducible (Table 2), 2. The amounts of intermixing in $MnBi_2Te_4$ are relatively small in comparison with $MnSb_2Te_4$.

On the other hand, for $MnSb_2Te_4$ there is a wide range of critical temperatures reported in the literature as shown in Table 4. As can be seen, not only different critical temperatures but even completely different magnetic ground states are reported. In order to characterize the magnetism of our samples, magnetization measurements as a function of temperature were performed as shown in Figure 3.

Sample S1 (Figure 3a) shows an irreversible behavior in ZFC and FC magnetization curves below 32 K at 100 Oe which is suppressed by increasing the applied magnetic field, finally disappearing at 1000 Oe, suggesting a soft ferromagnetic or ferrimagnetic behavior. In contrast, sample S2 (Figure 3b) evidences a more complex behavior. Whereas the magnetization initially increases by lowering temperature indicating ferro/ferrimagnetism like in S1, a feature around 18 K is observed, followed by a peak at ca 13 K, a signature for an antiferromagnetic spin alignment/component. Notably the transition temperature determined from the inflection point is much lower for S2 than for S1, indicating a weakening of the ferro/ferrimagnetic state.

As noted previously, EDX and PXRD revealed that S1 is phase pure while S2 is multi-phase. In that sense, the magnetic behavior observed in S1 can therefore be ascribed to $MnSb_2Te_4$ only. Ferromagnetic or ferrimagnetic behavior has also been reported in $MnSb_2Te_4$ in other sources as cited above, where they find the following compositions: $MnSb_{1.4}Te_4$, $T_C = 25$ K [14]; $Mn_{0.846(6)}Sb_{2.154(6)}Te_4$, $T_N = 19$ K

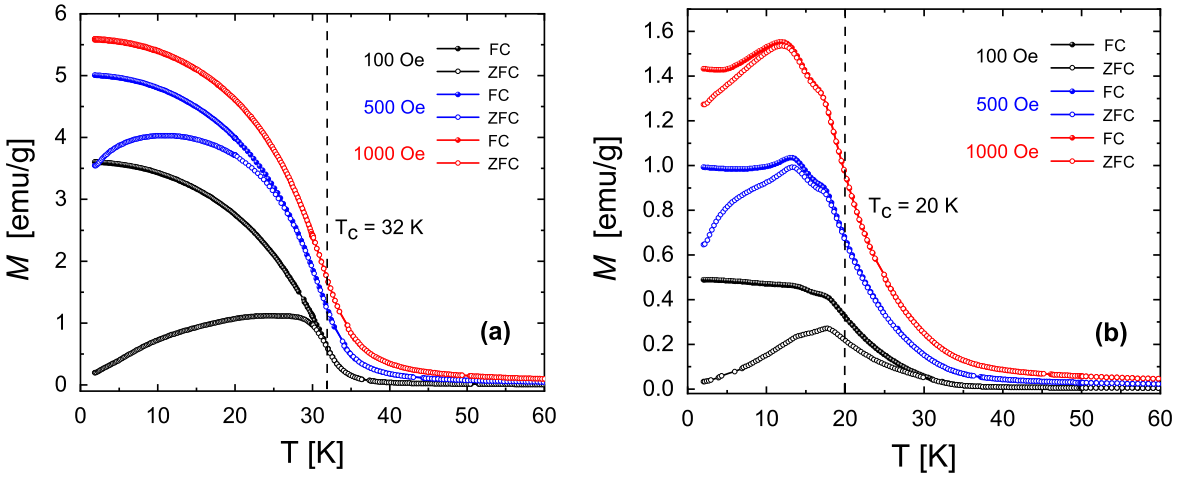

Figure 3: Temperature-dependent magnetization measurements of (a) S1 and (b) S2 powder samples obtained at various fields after field-cooled (FC) and zero-field-cooled (ZFC) procedures. The vertical dashed lines indicate the transition temperature T_C determined from the inflection point of the low field data.

or $Mn_{0.99(1)}Sb_{2.01(1)}Te_4$, T_C = 34 K, single crystal [13]; $Mn_{1.07}Sb_{1.9}Te_4$, T_C = 45–50 K, MBE thin films [16]. As evidenced, different amounts of intermixing and possible vacancies can lead to dramatic changes in the magnetic ordering transition. Our S1 hence excellently adds another data point to this collection of varying composition versus magnetic response. On the other hand, since S2 contains admixed phases that are magnetically active ($MnSb_4Te_7$ AFM with T_N = 13.5 K [27] and Mn-doped Sb_2Te_3 FM with transition temperatures between T_C = 9–17 K depending on amount of Mn in Sb_2Te_3 and publication [28–30]), the interpretation of its magnetic response becomes complex, since the influences from both additional phases contribution plus intermixing effects need to be disentangled.

As discussed above, there are various, albeit small, differences in terms of occupancies and amounts of elements that are present in the respective crystals. Referring back to the synthesis procedures for the two samples (see Section 2) and following the principle of Ockham's razor, we put forward the theory that small differences in synthetic conditions (annealing time and temperature) could be the key to tuning variances in occupancy. These findings are corroborated by similar reports from other groups [12–17], where especially Liu et al. [13] point out the correlation between synthesis temperature and intermixing. Thus it is possible to grow single crystals and phase pure powders of $MnSb_2Te_4$ with varying tempering routes and starting materials and we propose that $MnSb_2Te_4$ is not a line phase but exhibits a certain phase width.

While for $MnBi_2Te_4$ reported starting-material compositions vary (Bi_2Te_3-rich melts versus 1:1 MnTe:Bi_2Te_3 composition), the tempering profile has been the same in most reports as it is dictated by the high-temperature phase-stability interval. This is at stark contrast to the variability of synthesis conditions for $MnSb_2Te_4$. On one hand, the wide homogeneity range of $MnSb_2Te_4$ can lead to severe problems with reproducibility. On the other hand, the variability in $MnSb_2Te_4$ may give us more freedom to tailor its physical properties via the composition with the chance of driving the magnetic transition to higher temperatures and confining the magnetic order to ferromagnetism. Furthermore it opens broad possibilities to study the interplay between bulk magnetism and topological surface transport.

Acknowledgment: We would like to express our gratitude to Prof. Jan J. Weigand (TU Dresden) for giving us access to a Supernova single-crystal diffractometer, Prof. Thomas Doert for helpful discussions of the crystallographic data and to Mc.S. Ekaterina Vinokurova and Mc.S. Yiran Wang for conducting the EDX measurements.

Author contributions: All the authors have accepted responsibility for the entire content of this submitted manuscript and approved submission.

Research funding: This project has been supported by the Deutsche Forschungsgemeinschaft (DFG) through the Collaborative Research Center 1143 (Project ID 247310070) and the Würzburg-Dresden Cluster of Excellence ct.qmat (EXC 2147, Project ID 390858490). L.T.C. is funded by the Deutsche Forschungsgemeinschaft (DFG) – (Project ID 456950766).

Conflict of interest statement: The authors declare no conflicts of interest regarding this article.

References

1. Tokura Y., Yasuda K., Tsukazaki A. Magnetic topological insulators. *Nat. Rev. Phys.* 2019, *1*, 126–143.
2. Hasan M. Z., Kane C. L. Colloquium: topological insulators. *Rev. Mod. Phys.* 2010, *82*, 3045–3067.
3. Qi X. L., Zhang S. C. The quantum spin Hall effect and topological insulators. *Phys. Today* 2010, *63*, 33–38.
4. Chang C.-Z., Zhang J., Feng X., Shen J., Zhang Z., Guo M., Li K., Ou Y., Wei P., Wang L.-l., Ji Z.-Q., Feng Y., Ji S., Chen X., Jia J., Dai X., Fang Z., Zhang S.-C., He K., Wang Y., Lu L. Experimental observation of the quantum anomalous Hall effect in a magnetic topological insulator. *Science* 2013, *340*, 167–171.
5. Li H., Gao S.-Y., Duan S.-F., Xu Y.-F., Zhu K.-J., Tian S.-J., Liu Z.-T., Liu W.-l., Huang Y.-B., Li Y.-l., Liu Y., Zhang G.-B., Zhang P. Dirac surface states in intrinsic magnetic topological insulators. *Phys. Rev. X* 2019, *9*, 041039.
6. Tang P., Zhou Q., Xu G., Zhang S.-C. Dirac fermions in an antiferromagnetic semimetal. *Nat. Phys.* 2016, *12*, 1100–1105.
7. Shen J., Chen H., Huang L., Gao Y., Zheng Q., Zhang Y.-Y., Li G., Hu B., Qian G., Cao L., Zhang X., Fan P., Ma R., Wang Q., Yin Q., Lei H., Ji W., Du S., Yang H., Wang W., Shen C., Lin X., Liu E., Shen B., Wang Z., Gao H.-J. Localized spin-orbit polaron in magnetic Weyl semimetal $Co_3Sn_2S_2$. *Nat. Commun.* 2020, *11*, 5613.
8. Otrokov M. M., Klimovskikh I. I., Bentmann H., Estyunin D., Zeugner A., Aliev Z. S., Gaß S., Wolter A. U., Koroleva A. V., Shikin A. M., Blanco- Rey M., Hoffmann M., Rusinov I. P., Vyazovskaya A. Y., Eremeev S. V., Koroteev Y. M., Kuznetsov V. M., Freyse F., Sánchez-Barriga J., Amiraslanov I. R., Babanly M. B., Mamedov N. T., Abdullayev N. A., Zverev V. N., Alfonsov A., Kataev V., Büchner B., Schwier E. F., Kumar S., Kimura A., Petaccia L., Di Santo G., Vidal R. C., Schatz S., Kißner K., Ünzelmann M., Min C. H., Moser S., Peixoto T. R., Reinert F., Ernst A., Echenique P. M., Isaeva A., Chulkov E. V. Prediction and observation of an antiferromagnetic topological insulator. *Nature* 2019, *576*, 416–422.
9. Zeugner A., Nietschke F., Wolter A. U., Gaß S., Vidal R. C., Peixoto T. R., Pohl D., Damm C., Lubk A., Hentrich R., Moser S. K., Fornari C., Min C. H., Schatz S., Kißner K., Ünzelmann M., Kaiser M., Scaravaggi F., Rellinghaus B., Nielsch K., Hess C., Büchner B.,

Reinert F., Bentmann H., Oeckler O., Doert T., Ruck M., Isaeva A. Chemical aspects of the candidate antiferromagnetic topological insulator $MnBi_2Te_4$. *Chem. Mater.* 2019, *31*, 2795–2806.
10. Deng Y., Yu Y., Shi M. Z., Guo Z., Xu Z., Wang J., Chen X. H., Zhang Y. Quantum anomalous Hall effect in intrinsic magnetic topological insulator $MnBi_2Te_4$. *Science* 2020, *367*, 895–900.
11. Li H., Li Y., Lian Y.-K., Xie W., Chen L., Zhang J., Wu Y., Fan S. *Spin Glass State in Layered Compound $MnSb_2Te_4$*; Cornell University: New York, 2021.
12. Liu Y., Wang L. L., Zheng Q., Huang Z., Wang X., Chi M., Wu Y., Chakoumakos B. C., McGuire M. A., Sales B. C., Wu W., Yan J. Site mixing for engineering magnetic topological insulators. *Phys. Rev. X* 2021, *11*, 21033.
13. Murakami T., Nambu Y., Koretsune T., Xiangyu G., Yamamoto T., Brown C. M., Kageyama H. Realization of interlayer ferromagnetic interaction in $MnSb_2Te_4$ toward the magnetic Weyl semimetal state. *Phys. Rev. B* 2019, *100*, 195103.
14. Shi G., Zhang M., Yan D., Feng H., Yang M., Shi Y., Li Y. Anomalous Hall effect in layered ferrimagnet $MnSb_2Te_4$. *Chin. Phys. Lett.* 2020, *37*, 1–5.
15. Wimmer S., Sánchez-Barriga J., Küppers P., Ney A., Schierle E., Freyse F., Caha O., Michalička J., Liebmann M., Primetzhofer D., Hoffman M., Ernst A., Otrokov M. M., Bihlmayer G., Weschke E., Lake B., Chulkov E. V., Morgenstern M., Bauer G., Springholz G., Rader O. Mn-rich $MnSb_2Te_4$: a topological insulator with magnetic gap closing at high Curie temperatures of 45–50 K. In *Advanced Materials*; John Wiley & sons: Weinheim, 2021; p. 2102935.
16. Zhou L., Tan Z., Yan D., Fang Z., Shi Y., Weng H. Topological phase transition in the layered magnetic compound $MnSb_2Te_4$: spin-orbit coupling and interlayer coupling dependence. *Phys. Rev. B* 2020, *102*, 85114.
17. Ge W., Sass P., Yan J., Lee S. H., Mao Z., Wu W. Direct Evidence of Ferromagnetism in $MnSb_2Te_4$. *Phys. Rev. B* 2021, *103*, 134403.
18. Yan J. Q., Okamoto S., McGuire M. A., May A. F., McQueeney R. J., Sales B. C. Evolution of structural, magnetic, and transport properties in $MnBi_{2-x}Sb_xTe_4$. *Phys. Rev. B* 2019, *100*, 104409.
19. CrysAlis Pro, Technologies, *Oxford Diffraction*; Agilent Technologies UK Ltd: Yarnton, England, 2017.
20. Palatinus L., Chapuis G. Superflip – a computer program for the solution of crystal structures by charge flipping in arbitrary dimensions. *J. Appl. Crystallogr.* 2007, *40*, 786–790.
21. Petříček V., Dušek M., Palatinus L. Crystallographic computing system Jana2006: general features. *Z. Kristallogr.* 2014, *229*, 345–352.
22. Ding L., Hu C., Ye F., Feng E., Ni N., Cao H. Crystal and magnetic structures of magnetic topological insulators $MnBi_2Te_4$ and $MnBi_4Te_7$. *Phys. Rev. B* 2020, *101*, 1–6.
23. Yan J. Q., Zhang Q., Heitmann T., Huang Z., Chen K. Y., Cheng J. G., Wu W., Vaknin D., Sales B. C., McQueeney R. J. Crystal growth and magnetic structure of $MnBi_2Te_4$. *Phys. Rev. Mater.* 2019, *3*, 1–8.
24. Batsanov S. S. Van der Waals radii of the elements. *Inorg. Mater.* 2001, *37*, 871–885.
25. Orujlu E. N., Aliev Z. S., Amiraslanov I. R., Babanly M. B. Phase equilibria of the MnTe-Sb_2Te_3 system and synthesis of novel ternary layered compound - $MnSb_4Te_7$. *Phys. Chem. Solid State* 2021, *22*, 39–44.
26. Huan S., Zhang S., Jiang Z., Su H., Wang H., Zhang X., Yang Y., Liu Z., Wang X., Yu N., Zou Z., Shen D., Liu J., Guo Y. Multiple magnetic topological phases in bulk van der Waals crystal $MnSb_4Te_7$. *Phys. Rev. Lett.* 2021, *126*, 1–7.
27. Choi J., Lee H. W., Kim B. S., Choi S., Choi J., Song J. H., Cho S. Mn-doped V 2VI 3 semiconductors: single crystal growth and magnetic properties. *J. Appl. Phys.* 2005, *97*, 2–5.
28. Hor Y. S., Roushan P., Beidenkopf H., Seo J., Qu D., Checkelsky J. G., Wray L. A., Hsieh D., Xia Y., Xu S. Y., Qian D., Hasan M. Z., Ong N. P., Yazdani A., Cava R. J. Development of ferromagnetism in the doped topological insulator $Bi_{2-x}Mn_xTe_3$. *Phys. Rev. B Condens. Matter* 2010, *81*, 1–7.
29. Teng J., Liu N., Li Y. Mn-doped topological insulators: a review. *J. Semiconduct.* 2019, *40*. https://doi.org/10.1088/1674-4926/40/8/081507.

Supplementary Material: The online version of this article offers supplementary material (https://doi.org/10.1515/zkri-2021-2057).

Bionotes

Laura C. Folkers received her M.Sc. from ETH Zürich, Switzerland in 2015 and her Ph.D. from the faculty of engineering at Lund University, Sweden in 2019. Currently she is a postdoctoral fellow of the ct.qmat Cluster of Excellence at Technische Universität Dresden, Germany. She conducts her research in the group of assistant professor Anna Isaeva and focuses on synthesis and crystallographic studies of layered magnetic topological chalcogenides. The research group is active at the boundary of materials science and solid-state physics, and pursues design, inorganic synthesis and structural characterization of bulk van-der-Waals quantum materials, with topological insulators and frustrated magnets in the centre of attention. The group has developed at Technische Universität Dresden and Leibniz Institute for Solid State and Materials Research IFW-Dresden, Germany and is now in the process of relocating to the Institute of Physics at the University of Amsterdam, The Netherlands. Isaeva's group is the nodal point of a large collaborative research network exploring new topological materials.

Laura Teresa Corredor obtained her Ph.D. from the Universidad Nacional de Colombia in 2012, followed by postdoctoral researcher positions at the Universidade Federal de Pernambuco in Brazil and at Leibniz Institute for Solid State and Materials Research IFW-Dresden, Germany. After an assistant professorship at the Universidade Federal do Rio Grande do Norte in Brazil between 2017 and 2019, Dr. Corredor returned to IFW-Dresden, where she is currently conducting her research in the Thermodynamics Group headed by Dr. Anja Wolter-Giraud. The research interest of this group focuses in obtaining fundamental insights into the properties of emerging unconventional spin phases through thermodynamic methods like magnetometry, dilatometry and calorimetry in extreme conditions of low temperatures, high fields and high pressures. Particular focus is given to quantum magnets with reduced dimensionality, frustration and the interplay of spin, charge, structure and orbitals in complex transition metal oxide systems, as well as to explore the interplay between magnetism and superconductivity in unconventional high-temperature superconductors.